Role of chaos in one-dimensional heat conductivity

Jun-Wen Mao,[1,2] You-Quan Li,[1] and Yong-Yun Ji[1]
[1]*Zhejiang Institute of Modern Physics, Zhejiang University, Hangzhou 310027, People's Republic of China*
[2]*Department of Physics, Huzhou Teachers College, Huzhou 313000, People's Republic of China*
(Received 19 November 2004; published 23 June 2005)

We investigate the heat conduction in a quasi-one-dimensional gas model with various degrees of chaos. Our calculations indicate that the heat conductivity κ is independent of system size when the chaos of the channel is strong enough. The different diffusion behaviors for the cases of chaotic and nonchaotic channels are also studied. The numerical results of divergent exponent α of heat conduction and diffusion exponent β are consistent with the formula $\alpha=2-2/\beta$. We explore the temperature profiles numerically and analytically, which show that the temperature jump is primarily attributed to superdiffusion for both nonchaotic and chaotic cases, and for the latter case of superdiffusion the finite size affects the value of β remarkably.

DOI: 10.1103/PhysRevE.71.061202 PACS number(s): 44.10.+i, 05.45.−a, 05.70.Ln, 66.70.+f

I. INTRODUCTION

The low-dimensional microscopic dynamics of heat conduction has been an attractive question since the early 1900s. Much more attention has been paid to this problem in the past two decades due to the dramatic achievement in the application of miniaturized devices [1–6] which can be described by one-dimensional (1D) or 2D models. More and more numerical calculations are focused on the minimal requirements for a dynamical model whether or not Fourier's law holds [7–18]. A convergent heat conductivity was shown in ding-a-ling model [8,9], which is chaotic. The studies on the Lorentz gas model [10,11] (the circular scatters are periodically placed in the channel) of which the Lyapunov exponent is nonzero gave a finite heat conductivity which fulfills the Fourier law explicitly. Hence, chaos used to be regarded as an indispensable factor to normal heat conduction. Whereas the FPU model [12,13] indicated that the chaotic behavior is not sufficient to arrive at normal heat conduction, recently a series of billiard gas models [14,15,18] were devoted to explore the normal heat conduction of quasi-1D channels with zero Lyapunov exponent. However, the role of chaos in heat conduction has not been well understood. Additionally, the exponential stability and instability frequently coexist in the scatters of real systems. Thus the model with various degrees of chaos deserves further investigation from the microscopic point of view, and it will also be interesting to explore nonequilibrium stationary states and to determine the steady temperature field.

In this paper, we focus on the quasi-one-dimensional gas model, which is expected to describe a real two-dimensional system whose transverse size is much smaller than the longitudinal one such that the kinetic excitation in the transverse direction is frozen. The scatters in our model are the isosceles right triangle with a segment of circle substituting for the right angle. In this case, the edges of scatters are the combination of a line and a quarter of a circle. Such a channel is of chaos, which indicates exponential instability of microscopic dynamics. Our paper is organized as follows. In Sec. II, we introduce the model and investigate the degree of chaos for various channels with different arc-radius and channel height. In Sec. III, we study the heat transport behavior and the corresponding diffusive behavior by changing the radius of top arc and channel height. In Sec. IV, we investigate the nonequilibrium stationary state and determine the steady temperature field numerically. We also analyze the dependence of the temperature profile on diffusion exponent β and system size N theoretically. In Sec. V, we discuss the relation between our work and others and summarize our main conclusions.

II. THE MODEL

We consider a billiard gas channel with two parallel walls and a series of scatters. The channel consists of N replicate cells of length l and height h, and each cell is placed with two scatters as shown in Fig. 1. The scatter's geometry is an isosceles right triangle of hypotenuse a whose vertex angle is replaced by a segment of circle with radius R which is tangential to the two sides of the triangle. At the two ends of the channel are two heat baths with temperature T_L and T_R. Noninteracting particles coming from these heat baths are scattered by the walls and the straight lines as well as the arcs of the scatters in the channel.

For such a channel, the degree of chaos can be characterized qualitatively by the Poincaré surface of section (SOS) [19]. Suppose we take out one unit cell from the channel and close the two ends by straight walls. Then the problem becomes a billiard problem. A particle moves within the cell and causes an elastic collision with the mirrorlike boundary. We investigate the surfaces of section (s,v_τ) under different initial conditions. s is the length along the billiard boundary

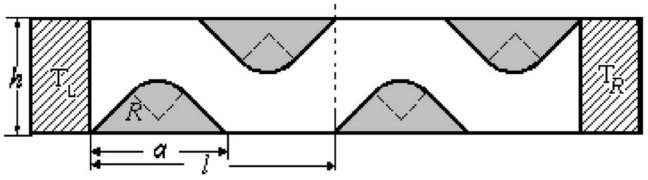

FIG. 1. The channel with N replicate cells. Here, $l=2.2$, $a=1.2$, h changes from 1.0 to 0.27, and R from 0 to 0.848 528 to ensure a quarter of a circle always.

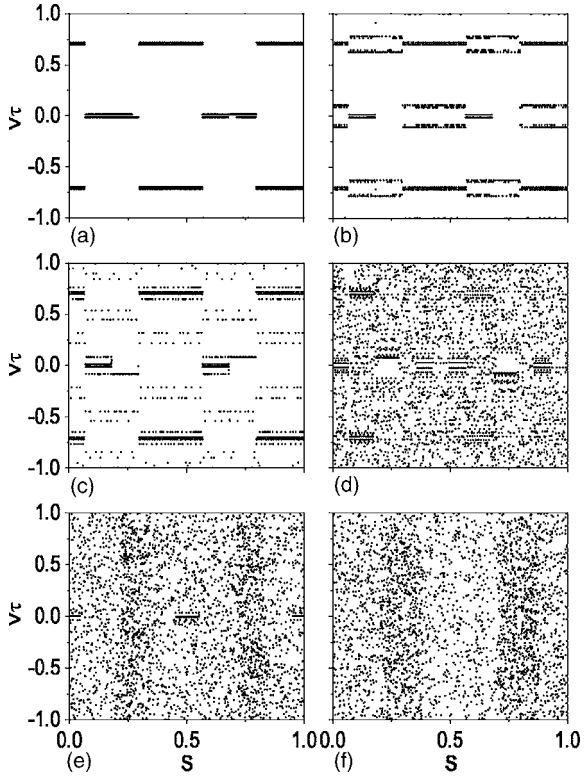

FIG. 2. Poincaré surface-of-section of the billiard problem. The billiard starts with an incident angle 0.8 and unit velocity. (a) $R=0$, $h=1.0$; (b) $R=0.001$, $h=1.0$; (c) $R=0.015$, $h=1.0$; (d) $R=0.1$, $h=1.0$; (e) $R=0.848\,528$, $h=1.0$; and (f) $R=0.848\,528$, $h=0.27$.

from the collision point to the reference point. v_τ is the tangential component of velocity with respect to the boundary at that point. The filling behavior of phase space shown in Fig. 2 indicates the degree of chaos. In case I, it is nonchaotic. The surface of section is regular and periodic, as shown in Fig. 2(a). As the radius R is increased from (a) to (e), the motion becomes more complex and the map becomes dense with points except for some regular islands. In Fig. 2(f), the regular parts disappear, which indicates strong chaos.

III. THE HEAT TRANSPORT AND DIFFUSION BEHAVIOR

To study the heat conduction of the model, the heat flux is investigated first. In calculating the heat flux, we follow Ref. [10]. For simplicity, the particles from the two heat baths are supposed to have definite velocities $\sqrt{2T_L}$ and $\sqrt{2T_R}$, respectively [14]. It is demonstrated by numerical simulation that the form of heat baths has no influence on the heat transport behavior in our system. We consider one particle colliding with a heat bath during a period of simulating time. The energy exchange $(\Delta E)_j$ at the jth collision with the heat bath is defined as

$$(\Delta E)_j = E_h - E_p, \tag{1}$$

where E_h denotes for the energy of the particle taken from the bath and E_p for that carried in the channel. For M collisions between the particle and the bath wall during the simulation time t, the heat flux is given by

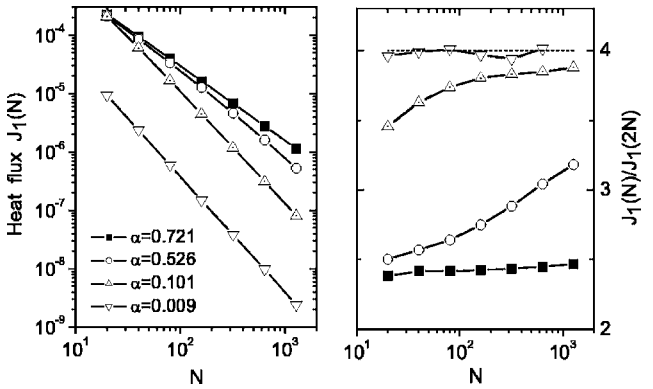

FIG. 3. The heat flux of a single particle versus system size ($N=20$, 40, 80, 160, 320, 640, and 1280) with the divergence exponent of heat conductivity $\alpha=0.721$, 0.526, 0.101, and 0.009 for four typical cases, respectively (left panel). The ratio of heat flux is $J_1(N)/J_1(2N)$ for different system sizes (right panel).

$$J_1(N) = \frac{\sum_{j=1}^{M} (\Delta E)_j}{t}. \tag{2}$$

As there is one heat carrier in each cell and the channel has N replicas, there are N particles in the whole channel. Summing over the heat flux of N heat carriers, we have $J_N(N)=NJ_1(N)$. Meanwhile, Fourier's law reads

$$J_N(N) = -\kappa \frac{dT}{dx} = \kappa \frac{T_L - T_R}{Nl}, \tag{3}$$

where κ refers to the heat conductivity which is determined by Eqs. (2) and (3),

$$\kappa \sim N^2 J_1(N). \tag{4}$$

We consider various cases by changing the radius R of the top arc of the scatters to investigate their effects on heat conduction. The heat flux of a single particle versus system size shown in Fig. 3 occurs in four typical cases. Case I: the ■ studies for $R=0$, $h=1.0$; case II: the ○ for $R=0.001$, $h=1.0$; case III: the △ for $R=0.848\,528$, $h=1.0$; and case IV: the ▽ for $R=0.848\,528$, $h=0.27$, respectively. The total cell numbers are chosen as $N=20$, 40, 80, 160, 320, 640, and 1280, respectively. After a sufficiently long period of simulation time, the heat flux approaches a constant value. Clearly, the value of heat flux decreases with increasing R for the same size. Remarkably, there is a 20 times difference of heat flux between case III and case IV, which indicates that smaller height suppresses the heat flux greatly. Thus, it appears that the value of heat flux can be adjusted in this way in designing heat-control devices. Furthermore, our calculations, show that the heat-flux dependence on N exhibits faint nonlinearity, although the curve looks linear for all cases except case IV in the log-log scale.

In order to observe the deviation from the line, which arises from the finite-size effect, we calculate the ratio of heat flux versus system size for various radii. The data for the aforementioned four cases are plotted in the right panel of Fig. 3, from which one can see that both the increasing of the system size and of the arc radius bring the ratio an up-

ward tendency to the value 4, which ensures the Fourier law. In case I, where $R=0$, there is only a slight increase for the ratio around 2.4, whereas the ratio rises drastically along with the increasing of systems size even if the radius R is merely 0.001 (case II). When $R=0.848\,528$ (case III), the scatters become a full segment of a quarter circle. The ratio also rises drastically at first and gradually after $N>160$ in this case. In both cases II and III, it seems to approach distinct asymptotic values which are all different from that for normal conduction. This implies that a smaller degree of chaos is insufficient to bring about a normal heat conduction, although the increasingly chaotic degree makes the divergent exponent of heat conduction smaller. In case IV, we maintain the scatters at radius $R=0.848\,528$ and reduce the height h from 1.0 to 0.27. In this strongly chaotic case, the ratio fluctuates around the value 4 (dotted line), which means that Fourier law is obeyed.

It is known that the normal heat conduction happens when $\alpha=0$, which indicates that the heat conductivity is independent of system size, and the anomalous heat conduction corresponds to the case of $\alpha>0$. The heat conductivity κ we calculated can be given by $\kappa\sim N^{\alpha}$ with $\alpha\gtrsim 0$ despite the heat-flux ratio having a different increase in asymptotic value for all cases (except case IV).

We calculate α at the range of system sizes N from 20 to 1280 by averaging over many realizations for various radii R at fixed channel height $h=1.0$, and the plot of the dependence of α on R is shown in Fig. 4(a). One can see that α descends from 0.721 through 0.526 to 0.092 if R increases from 0 to 0.848 528 for a fixed height $h=1.0$. Clearly, the α descends rapidly for small radius (e.g., $R=0.001$ in case II) and slowly for larger ones. This illustrates that the appearance of an arc on the top of the scatter suppresses the divergent exponent α drastically. If the channel height h for fixed $R=0.848\,528$ is changed from 1.0 to 0.27, the α is found to diminish to 0.009. Therefore, the κ appears to be independent of system size and the Fourier law holds in this case.

Since the characteristic of heat transport is found being closely related to the diffusion behavior [14,15,18,20–22], we investigate the diffusion property for the above cases subsequently. For a particle starting at the origin at time $t=0$ and diffusing along x direction, the mean square displacement $\langle[x(t)-x(0)]^2\rangle$ characterizes its diffusion behavior. For normal diffusion, the Einstein relation of $\langle[x(t)-x(0)]^2\rangle=Dt$ holds, where D is diffusion coefficient. If the mean-square displacement does not grow linearly in time, i.e., $\langle[x(t)-x(0)]^2\rangle=Dt^{\beta}$, we refer to anomalous diffusion. Recently, the connection between anomalous diffusion and corresponding heat conduction in a 1D system was discussed hotly [20–22]. We plot the mean-square displacement versus time t in Fig. 4(c) for the aforementioned four cases. Note that 10^5 particles were put at the center of the channel where $x=0$ with unit velocity and random direction in the simulations. The top solid line and the bottom dash-dot line are precisely straight in the whole simulation period ($t=10^5$), which corresponds to case I (nonchaotic) and case IV (strong chaotic), respectively. We obtain $\beta=1.628$ for case I, which corresponds to $\alpha=0.721$, and $\beta=1.001$ to $\alpha=0.009$ for case IV. Beyond these two cases, the curves remain asymptotically

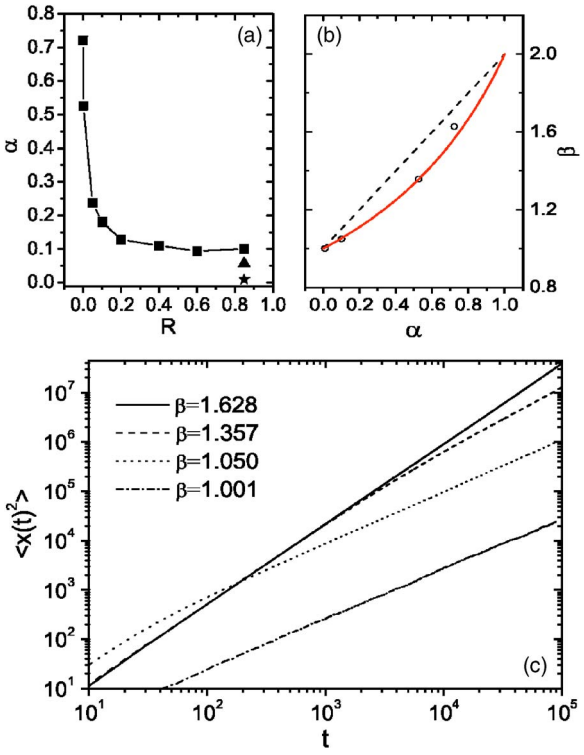

FIG. 4. (Color online) (a) Conductivity divergence exponent α vs circular radius R. The ■ refers to the magnitude of α for $h=1.0$, $R=0$, 0.001, 0.05, 0.1, 0.2, 0.4, 0.6, and 0.848 528; the ▲ for $h=0.5$ and $R=0.848\,528$; the ★ for $h=0.27$ and $R=0.848\,528$ has the value of 0.009. (b) The relation between β and α, where the circle is the numerical result, the solid line is of $\alpha=2-2/\beta$ [20], and the dashed line is the result of Ref. [22]. (c) Log-log plot of mean-square displacement $\langle x(t)^2\rangle$ vs time t. The curves from top to bottom on the right correspond to cases I, II, III, and IV, respectively. The ensemble has 10^5 particles starting from the center of the channel at time $t=0$, where $x=0$ with the unit velocity and random direction.

linear at large time t with diffusion exponent β between the values of above two cases. The best fits of the slope give $\beta=1.357$, which corresponds to $\alpha=0.526$ for case II and $\beta=1.050$ to $\alpha=0.101$ for case III, respectively. The relation between divergent exponent α and diffusion exponent β fits the relation of $\alpha=2-2/\beta$ proposed by Li and Wang in Ref. [20], as is plotted in Fig. 4(b), whereas Denisov *et al.* presented another connection of α with β on the basis of the Lévy walk model [22]. More details about the origin of the discrepancy between the above two relations can be found in Ref. [21].

As different diffusion behaviors are likely related to the trajectory characteristics of the particle propagation, we investigate the PDF $\psi(|\delta x|)$ of the flight distance $|\delta x|$ in the x direction between two consecutive collisions with the scatters. After a long time for adequate collisions in the channel, the PDFs for the aforementioned four cases, shown in Figs. 5(a)–5(d), respectively, take on completely different forms for different cases. In case I, the discrete values of probability indicate that the trajectories have abundant periodicity, which is almost identical to larger system size. The maximum value of PDF appears when $|\delta x|=0.447$, and the typical

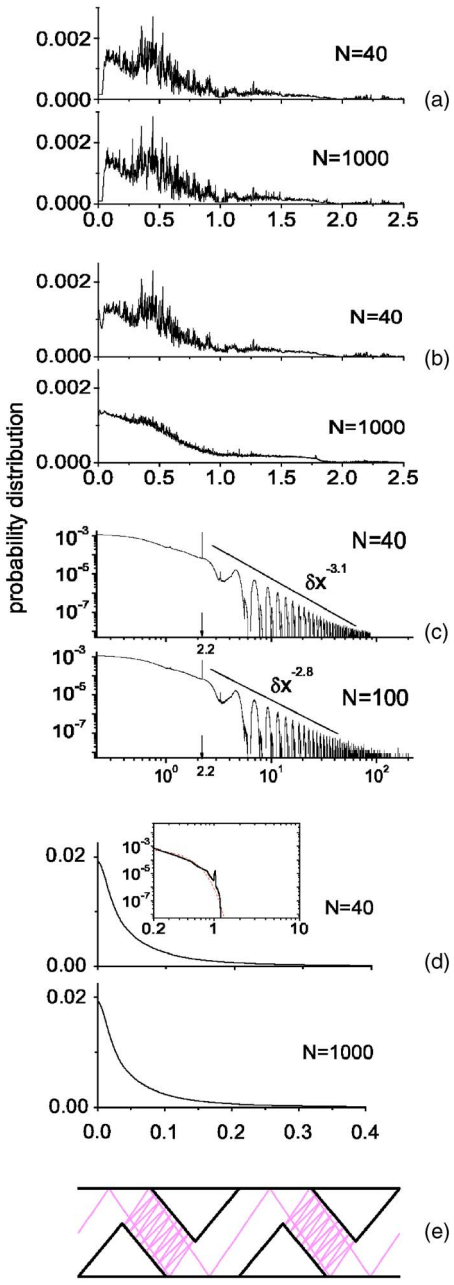

FIG. 5. (Color online) (a), (b), (c), and (d) The PDFs of the flight distance $|\delta x|$ between two consecutive collisions for the four cases I, II, III, and IV, respectively. N represents the system size. Note that the log-log scale is used in (b) and the inset of (d) where Gaussian distribution (dashed line) is in comparison to the numerical PDF (solid line). (e) The typical trajectory (thin lines) with periodicity in the case of $R=0, h=1.0$.

trajectory is plotted in Fig. 5(e), which shows explicitly that the parallel passage makes the periodic trajectory possible, and the particles are easier to propagate along the channel with fewer collisions. It is superdiffusion in this case. In case II, only the smaller system size has explicit periodicity. With the system size growing, the periodicity is destroyed by the collisions with the segment of circle time and time. The PDF gets smoother in this case. In case III, the periodicity happens only for large flight distance $|\delta x|$ with a very small number of families. Note that the maximum of PDF corresponds to the value $|\delta x|$ of 2.2, which is just the length of a cell, and the PDF decays in power law. In this case, it requires more collisions and takes more time for the particles to escape a certain region. Thus the propagation is suppressed but is still of superdiffusion. The normal diffusion takes place when the particles are scattered by a sufficiently large density of hyperbolic scatters (case IV). Consequently, the strong chaos presents the trajectory of heat carriers with more aperiodicity. The PDF takes on its characteristic form, which has a Gaussian tail as shown in the inset of Fig. 5(d).

Thus, the propagation modes are responsible for the diffusion behavior. The abundance of the aperiodicity of the trajectory is characteristic of a chaotic channel and may also play a crucial role in normal diffusion. In other words, if the trajectory in a certain system brings about the aperiodicity due to some other mechanisms, such as in the polygonal billiard gas model [15], the normal diffusion behavior occurs.

IV. THE CALCULATION OF TEMPERATURE FIELD

We calculate the temperature field following the approach proposed in Ref. [10]. The temperature of the ith cell is defined by averaging the kinetic energy over all visits into the cell,

$$T_i = \langle E_i \rangle = \frac{\sum_{j=1}^{m} t_j E_{ij}}{\sum_{j=1}^{m} t_j}, \tag{5}$$

where t_j denotes the time spent within the cell in the jth visit, and m is the total number of visits. For sufficiently large m, we expect a steady temperature profile, and this is indeed verified in our calculations for a total of 10^{10} visits. The temperature profiles we obtained are plotted in Fig. 6. It is worthwhile to point out that the steady temperature profiles between nonchaotic and chaotic systems are quite different in the thermodynamic limit, which is due to the different diffusion behaviors as shown in Fig. 4(c). As case I is nonchaotic and has uniform diffusion exponent β, the temperature profiles keep almost the same shape for different system sizes. At the two ends of the channel there are large temperature jumps which play an important role in the Fourier transport and dynamics of the system [23]. These jumps arise from the boundary heat resistance, which usually appears when there is a heat flux across the interface of the two adjacent materials. In cases II and III, which are chaotic and have asymptotically decreasing β, there also exists boundary heat resistance. Unlike in case I, the temperature jump here is smaller and diminishes when the system size grows. For larger size there is almost no temperature jump which corresponds to a nearly linear temperature profile. Both the larger system size N and the arc radius lead to the increase of chaos degree which is responsible for the decrease of diffusion exponent β ($\geqslant 1$). In case IV, which is strongly chaotic, the temperature profiles are almost linear for various system

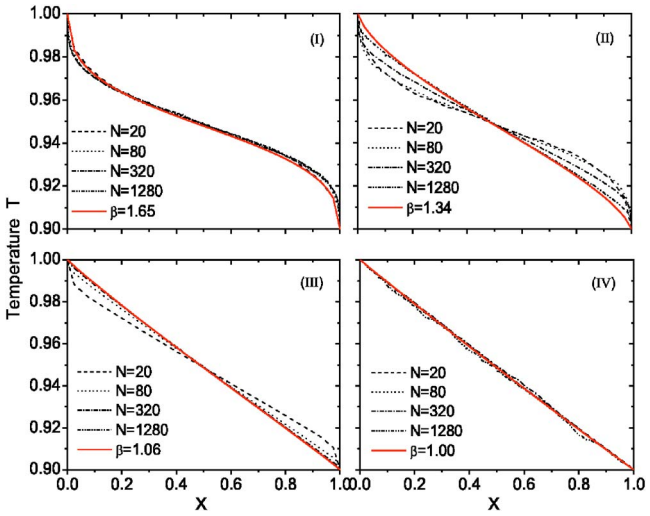

FIG. 6. (Color online) Numerical results of temperature profiles for $T_L=1.0$, $T_R=0.9$, and sizes $N=20$ (dash), 80 (dot), 320 (dash dot), and 1280 (dash dot dot), respectively. The four panels refer to (I) $R=0$, $h=1.0$; (II) $R=0.001$, $h=1.0$; (III) $R=0.848\,528$, $h=1.0$; and (IV) $R=0.84\,528$, $h=0.27$. The solid lines correspond to the best fits for the numerical temperature profile at $N=1280$ with Eq. (8), giving the analytical values β with 1.65, 1.34, 1.06, and 1.00 for the above four cases, respectively.

sizes we considered, corresponding to the normal heat conduction.

We estimate the temperature profiles from the average point of view. Considering the incident particles from the left heat bath (where $x=0$) propagating along the x axis to the right end, we suppose that a reflecting boundary is placed at the origin of the x axis and an absorbing one at the other end. When $2 \geqslant \beta \geqslant 1$, we assume that the mean density $n_L(x)$ of the particles at site x in the steady state is proportional to $(1-x)^\gamma$ with $\gamma=(2/\beta-1)\beta^{3/2}$, where we set $x=i/N$. Under this assumption, we have $n_L(x)\sim 1-x$ [10] when $\beta=1$ (normal diffusion) and $n_L(x)\sim$ const when $\beta=2$ (ballistic diffusion). The conservation of particle number requires

$$n_L(x) \sim \frac{(1-x)^\gamma}{D_L}, \tag{6}$$

where D_L is the diffusion coefficient. Likewise, for a particle propagating from right to left, we have

$$n_R(x) \sim \frac{x^\gamma}{D_R}. \tag{7}$$

We assume $D_L=T_L^{\beta/2}$ and $D_R=T_R^{\beta/2}$. Thus, if $2 \geqslant \beta \geqslant 1$, the temperature is given by

$$T(x) = \frac{T_L n_L(x) + T_R n_R(x)}{n_L(x) + n_R(x)} = \frac{T_L T_R^{\beta/2}(1-x)^\gamma + T_L^{\beta/2} T_R x^\gamma}{T_L^{\beta/2} x^\gamma + T_R^{\beta/2}(1-x)^\gamma}, \tag{8}$$

where $\gamma=(2/\beta-1)\beta^{3/2}$.

As shown in Figs. 6 and 7, the analytical results (in solid lines) are in good agreement with the numerical ones except those at the two ends of the channel for superdiffusion cases.

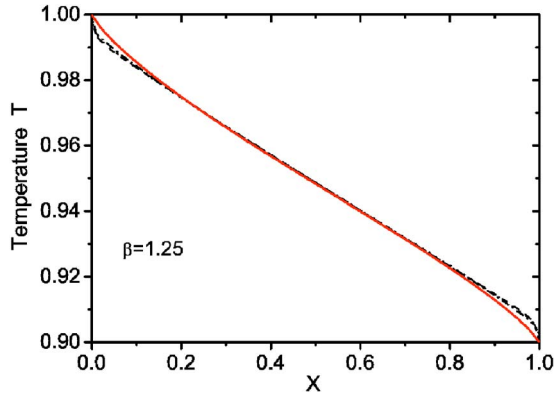

FIG. 7. (Color online) Numerical results of the temperature profile in comparison to the analytical results. The numerical temperature profiles with $R=0.848\,528$, $N=40$ (dash); $R=0.1$, $N=80$ (dot); and $R=0.05$, $N=160$ (dash dot) at $h=1.0$ almost share the same shape. The solid line (the upper on the left) is the plot of Eq. (8) with $\beta=1.25$.

These deviations are likely due to the different boundary conditions we used in the numerical calculations and in deducing Eq. (8). Furthermore, the value of β, obtained by the best fits for the numerical temperature profile at $N=1280$ with Eq. (8), agrees strongly with the simulated result for the aforementioned four cases. One can see clearly from Eq. (8) that the temperature profiles are closely related to the diffusion exponent β, namely, the case with the smaller diffusion exponent tends to have a smaller temperature jump. Accordingly, it is not unexpected that different chaotic cases may share the same temperature profile if they have the identical diffusion exponent β, as shown in Fig. 7, and the case with the smaller diffusion exponent requires a smaller system size to achieve the same temperature profile. Moreover, our calculations show that the results of Eq. (8) are consistent with the numerical ones even in a larger temperature gradient. Thus, the temperature profile is mostly dependent on the diffusion behavior, which is remarkably affected by the finite-size effect for chaotic cases of superdiffusion.

V. DISCUSSION AND CONCLUSION

In summary, we have investigated the role that chaos plays in heat conduction by the billiard gas channel. We have demonstrated that the degree of dynamical chaos is enhanced by increasing the arc radius or the system size for the chaotic channel, and the mass and heat transport behavior is significantly related to the degree of dynamical chaos of a channel. The stronger the chaos is, the closer to normal transport behaviors the model seems to be. Furthermore, our numerical results of two exponents α and β for both nonchaotic and chaotic cases satisfy the formula $\alpha=2-2/\beta$ when $\beta \geqslant 1$ [20]. We also discussed the microscopic dynamics by the PDF of flight distance in the x direction. It seems that the aperiodicity of the trajectory plays an important role in diffusion behavior. Finally, our results showed that the temperature jumps at both ends of the channel depend mostly on the diffusion property for both nonchaotic and chaotic channels,

and the finite-size effect is more crucial for chaotic ones.

Although the billiard model with noninteracting particles is a drastically simplified model, it is applicable for capturing the underlying dynamics of many systems and has in fact been realized to a good approximation in experiments, such as the experiments on antidot superlattices [24] and those involving semiconductor microjunctions [25]. In those systems, the carriers can be regarded as ideal noninteracting particles since their Fermi wavelength is usually smaller than the characteristic size of the lattice or junction. Moreover, the Lorentz model [26] has been used to explore the link between electrical conductivity and diffusion successfully.

We have used δ-function velocity distribution for the heat bath in our numerical calculations. One may argue that the heat bath with Gaussian velocity distribution is more practical for a laboratory thermostat [10,18,26]. We have calculated the temperature profiles and heat flux using the Gaussian-type heat bath, and we found that the heat-transport behavior in our system is not affected by the heat baths. So we take on δ-function velocity distribution for simplicity. In some cases, i.e., in quantum systems, a Gaussian thermostat may be more appropriate.

It is worthwhile to discuss the relation between our work and others in this field. Alonso *et al.* [10] investigated the 1D Lorentz gas model full of periodically distributed half-circular scatters. By defining the heat conductivity and temperature field as a statistical average over time on the hypothesis of local thermal equilibrium, the Fourier law holds in this case, and a linear gradient is given for a quite small temperature difference. Our work starts from the same approach but different scatter geometry is taken into account. Thus it is not surprising that our work has some overlap with theirs in spirit. However, we pay much more attention to the role played by the different degrees of dynamical chaos in heat conduction. As a result, our intensive calculations extended the results in Ref. [10] and concluded that only sufficiently strong chaos results in normal diffusion, thus the normal heat transport.

Li *et al.* [14] presented the dependence of heat conductivity on system size and the temperature profile in a channel with zero Lyapunov exponent where the right triangle scatters are periodically distributed. In this case, the exponent stability leads to abnormal transport behavior. Clearly, their result is the nonchaotic limit of our model.

ACKNOWLEDGMENTS

We would like to thank B. Li for providing Ref. [21] prior to publication and for helpful discussion. The work is supported by NSFC Grants No. 10225419 and No. 90103022.

[1] H. Forsman and P. Anderson, J. Chem. Phys. **80**, 2804 (1984).
[2] L. Taillefer, B. Lussier, R. Gagnon, K. Behnia, and H. Aubin, Phys. Rev. Lett. **79**, 483 (1997).
[3] T. S. Tighe, J. M. Worlock, and M. L. Roukes, Appl. Phys. Lett. **70**, 2687 (1997).
[4] J. Hone, M. Whitney, C. Piskoti, and A. Zettl, Phys. Rev. B **59**, R2514 (1999).
[5] P. Kim, L. Shi, A. Majumdar, and P. L. McEuen, Phys. Rev. Lett. **87**, 215502 (2001).
[6] G. Zhang and B. Li, e-print cond-mat/0403393.
[7] S. Lepri, R. Livi, and A. Politi, Phys. Rep. **377**, 1 (2003), and references therein.
[8] G. Casati, J. Ford, F. Vivaldi, and W. M. Visscher, Phys. Rev. Lett. **52**, 1861 (1984).
[9] H. A. Posch and W. G. Hoover, Phys. Rev. E **58**, 4344 (1998).
[10] D. Alonso, R. Artuso, G. Casati, and I. Guarneri, Phys. Rev. Lett. **82**, 1859 (1999).
[11] C. Mejia-Monasterio, H. Larralde, and F. Leyvraz, Phys. Rev. Lett. **86**, 5417 (2001).
[12] H. Kaburaki and M. Machida, Phys. Lett. A **181**, 85 (1993).
[13] S. Lepri, R. Livi, and A. Politi, Phys. Rev. Lett. **78**, 1896 (1997).
[14] B. Li, L. Wang, and B. Hu, Phys. Rev. Lett. **88**, 223901 (2002).
[15] D. Alonso, A. Ruiz, and I. de Vega, Phys. Rev. E **66**, 066131 (2002); Physica D **187**, 184 (2004).
[16] O. Narayan and S. Ramaswamy, Phys. Rev. Lett. **89**, 200601 (2002).
[17] S. Lepri, R. Livi, and A. Politi, Europhys. Lett. **43**, 271 (1998).
[18] B. Li, G. Casati, and J. Wang, Phys. Rev. E **67**, 021204 (2003).
[19] Jose L. Vega, Turgay Uzer, and Joseph Ford, Phys. Rev. E **48**, 3414 (1993).
[20] B. Li and J. Wang, Phys. Rev. Lett. **91**, 044301 (2003).
[21] B. Li *et al.*, Chaos **15**, 015121 (2005).
[22] S. Denisov, J. Klafter, and M. Urbakh, Phys. Rev. Lett. **91**, 194301 (2003).
[23] K. Aoki and D. Kusnezov, Phys. Rev. Lett. **86**, 4029 (2001).
[24] D. Weiss, M. L. Roukes, A. Menschig, P. Grambow, K. von Klitzing, and G. Weimann, Phys. Rev. Lett. **66**, 2790 (1991); R. Schuster, K. Ensslin, J. P. Kotthaus, G. Bohm, and W. Klein, Phys. Rev. B **55**, 2237 (1997).
[25] C. M. Marcus, A. J. Rimberg, R. M. Westervelt, P. F. Hopkins, and A. C. Gossard, Phys. Rev. Lett. **69**, 506 (1992); C. M. Marcus, R. M. Westervelt, P. F. Hopkins, and A. C. Gossard, Chaos **3**, 643 (1993); M. W. Keller, O. Millo, A. Mittal, D. E. Prober, and R. N. Sacks, Surf. Sci. **305**, 501 (1994); J. Cserti, G. Vattay, J. Koltai, F. Taddei, and C. J. Lambert, Phys. Rev. Lett. **85**, 3704 (2000).
[26] N. I. Chernov, G. L. Eyink, J. L. Lebowitz, and Ya. G. Sinai, Phys. Rev. Lett. **70**, 2209 (1993).